AO3 Proposer's Guide
VLBI Space Observatory Programme

Prepared by the

VSOP Science Operations Group

Institute of Space and Astronautical Science

2 September 1999

Proposals Due: Friday, 1 Oct 1999

Abstract

This guide provides the technical information necessary to write a proposal for scientific observations with the VLBI Space Observatory Programme (VSOP). Whereas the third VSOP Announcement of Opportunity (AO3) provides an overview of the VSOP mission and the proposal process, this guide provides technical details on many mission components and activities. These components include the VSOP spacecraft (HALCA), the ground radio telescopes, tracking stations, correlators and user support facilities of the VSOP mission.

Editor: D. W. Murphy

Contents

1 VSOP Mission Description **4**

2 HALCA Antenna **5**

3 HALCA Science Subsystem **5**

4 HALCA Constraints **8**
4.1 Sun . . . 8
4.2 Moon . . . 8
4.3 Earth . . . 8
4.4 Eclipse . . . 9
4.5 Tracking Network . . . 9
4.6 Spacecraft Telemetry Horizon Mask . . . 9
4.7 Changing Sources . . . 10
4.8 On-board Command Memory . . . 10

5 HALCA Orbit **10**
5.1 Definition of the Orbital Elements . . . 10
5.2 Orbit Normal and (u,v) Coverages . . . 11
5.3 Precession of the Orbital Elements . . . 12
5.3.1 Impact of Ω Precession . . . 13
5.3.2 Impact of ω Precession . . . 13

6 HALCA Tracking Network **13**

7 Ground Radio Telescopes **15**

8 VLBI Recorders and Correlators **15**
8.1 VLBI Recorders . . . 15
8.2 Correlators and Tape Copiers . . . 15

9 Observational Capabilities of the VSOP Mission **17**
9.1 Resolution . . . 19
9.2 Baseline Sensitivity . . . 19
9.3 Fringe Fitting Signal to Noise Ratio . . . 20
9.4 Fringe Detection Limit . . . 21
9.5 Estimated Correlated Flux Density . . . 21
9.5.1 Using the Source Size . . . 21
9.5.2 Using the Source Brightness Temperature . . . 22
9.6 Field of View . . . 22
9.6.1 Bandwidth Smearing . . . 23
9.6.2 Time Average Smearing . . . 23
9.7 Imaging Sensitivity . . . 24
9.8 Dynamic Range . . . 25
9.9 Typical VSOP Observations . . . 26
9.10 Polarimetry . . . 26

9.11 Spectral Line Observations 26
9.12 Pulsar Observations 27
9.13 Phase-referencing 27

10 HALCA Calibration **28**

11 VSOP Simulation Software **28**

12 VSOP Data Analysis **28**
12.1 Data Reduction 28
12.2 User Support Facilities 29

13 VSOP Proposal Help **29**

14 Web Site for Additional Information **30**

15 Acknowledgments **30**

A References **31**

B Acronyms and Abbreviations **32**

C HALCA Mass and Power Budgets **33**

D Change Log **34**

List of Figures

1 VSOP Spacecraft 4
2 HALCA Science Subsystem 6
3 HALCA Eclipse History. 9
4 Example All-Sky (u,v) Plot 12
5 Example (u,v) Plot as a Function of Time 14
6 Comparison of ground-space and ground-only 1928+738 images 18
7 (u,v) coverage for 1928+738 observation 18

List of Tables

1 HALCA Science Subsystem 7
2 HALCA Observing Modes 7
3 HALCA Orbital Elements 11
4 HALCA Tracking Network 14
5 Ground Radio Telescopes and VLBI Networks 16
6 Correlator Properties 17
7 Tape Copiers at the VSOP Correlator 17
8 HALCA Coherence Times 20
9 Satellite Mass Budget 33
10 Satellite Power Budget 33

1 VSOP Mission Description

The VLBI Space Observatory Programme (VSOP) is a project of the Japanese Institute of Space and Astronautical Science (ISAS) in close collaboration with the Japanese National Astronomical Observatory (NAO). In addition, a number of organizations around the world are providing facilities and other support to the VSOP mission. The VSOP Science Operations Group (VSOG) is responsible for the day-to-day operation and management of the VSOP mission and is comprised of members from ISAS and NAO, with support from other individuals and agencies.

During its development HALCA was referred to as MUSES-B as it was the second in the series of ISAS's Mu Engineering satellites. However, after its successful launch on 12 February 1997 by the first launch of the M-V rocket, MUSES-B was renamed HALCA (Highly Advanced Laboratory for Communications and Astronomy). The HALCA spacecraft, as shown in Figure 1, has an 8 m diameter antenna and is expected to have a lifetime of 3-5 years. The mass and power budgets of the spacecraft are presented in Appendix C (Tables 9 and 10). HALCA is in a 6.3 hour orbit with an apogee height of 21,400 km (see §5 for more details on the orbit). The precession of the spacecraft's orbit allows good (u,v) coverage to be obtained for all parts of the sky for at least some epochs during the mission lifetime. The apogee height produces baselines to ground radio telescopes up to three times longer than on the Earth, while the perigee height of 560 km is low enough to fill the aperture without an annular gap between ground-ground and ground-space baselines. Typically, an observation during General Observing Time (GOT) lasts between 7–14 hours, although various constraints result in the loss of ground-space VLBI data for some part of each observation.

As stated in the third VSOP Announcement of Opportunity it is not possible to apply for 22 GHz observations during the period covered by the third AO. Consequently this guide concentrates on the characteristics of the VSOP mission at 1.6 and 5 GHz.

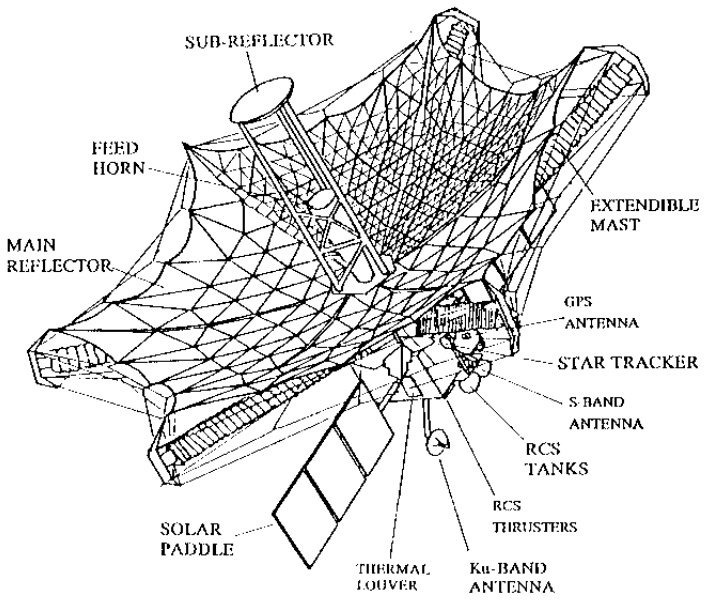

Figure 1: Diagram of the HALCA Spacecraft.

2 HALCA Antenna

The main HALCA antenna is a Cassegrain design with a three-waveband coaxial feed at the focus. Both the primary and secondary reflectors of the antenna were deployed in orbit. The primary reflector is composed of a thin mesh fixed in position by a set of cables attached to a support structure. The aperture has an area of 50.1 m^2, equivalent to an 8 m diameter reflector. The lower aperture efficiency at 1.6 GHz compared to 5 GHz (see Table 1) is primarily due to a large spillover loss at 1.6 GHz due to the limited size of the sub-reflector.

3 HALCA Science Subsystem

The HALCA science subsystem, a block diagram of which is shown in Figure 2, processes the radio astronomy signal as follows. After a quarter wave plate combines the two orthogonal linear polarizations into LCP, the received radiation is sent down a coaxial cable in the case of the 1.6 GHz and 5 GHz bands, and a waveguide in the case of the 22 GHz to the Low Noise Amplifiers (LNAs). After launch it was discovered that there is a very high attenuation ($\approx$10 dB) between the feed and the 22 GHz LNA. This is the reason that the 22 GHz performance of HALCA is well below pre-launch expectations and why no 22 GHz observations may be proposed for General Observing Time. One theory for this high attenuation is that the waveguide was damaged during launch. At both 1.6 and 5 GHz the LNAs have receiver noise temperatures of $\approx$ 35–40 K and gains of $\approx$ 35–40 dB. Unlike the case for ground-based VLBI antennas, at 1.6 and 5 GHz there are both relatively large feed losses ($\approx$ -0.6 dB) and coaxial cable ($\approx$ -0.2 dB) losses between the feed and the LNAs, which are located on a plate that lies directly below the feed. Associated with these losses is a large contribution ($\approx$ 40–55 K) to the overall HALCA system temperature. The physical temperatures of the LNAs vary from -24°C to $+13$°C. The rest of the science subsystem is located on a solar panel side of the spacecraft main body, which is a good location for passive cooling of various components.

After the LNAs, the signals from each RF band are down-converted to IF, split into two paths, and sent to the IF switch. Two of the six input signals (two from each RF band), which in normal modes of operation will be from the same RF band, are then sent to two separate video converters. These two channels are referred to as channel A and channel B. Each video converter is an image rejection mixer (IRM) which converts the IF signal to baseband (0–32 MHz) as well as rejecting the lower side band image frequencies. The LO frequency for each of the two video converters can be chosen in integral MHz steps and are independently set.

After the video converters, the A and B channel signals each pass through either 16-MHz or 32-MHz low pass filters, depending on which HALCA observing mode has been selected. At this stage the A and B channel signal levels are sampled by square law detectors, the 12-bit digital outputs of which are sent to the main spacecraft computer, the data handling unit (DHU), to be subsequently sent down to the ground in the VLBI data headers. These power levels are used to determine the HALCA system temperature and to monitor the sampler power levels. After this point, the A and B channel signals are one- or two-bit digitized, QPSK encoded onto the 14.2 GHz Ku-downlink carrier, further amplified, and sent to the Ku-band link antenna for transmission to a tracking station on the ground. The data rate of the downlink signal is 128 Mbps. The steerable Ku-band link antenna has a diameter of 45.5 cm and is located on a boom to improve tracking station communication.

HALCA does not have an on-board hydrogen maser frequency standard, but receives its reference signal from the ground as a 15.3 GHz tone derived from a hydrogen maser at a tracking station. This 15.3 GHz tone is received by the same Ku-link antenna that is used to transmit the 14.2 GHz downlink. The 15.3 GHz tone is sent to the Ku-band receiver, whose function is to search for, detect, and convert this tone into the fundamental 50 MHz reference signal for the spacecraft. The measured phase residuals in the two-way link signal are used to correct the spacecraft clock and oscillators at the correlator.

HALCA system temperatures are measured using noise diodes (one for each frequency band). On/off power ratios and a model for the noise powers enables the system temperatures in both channels to be

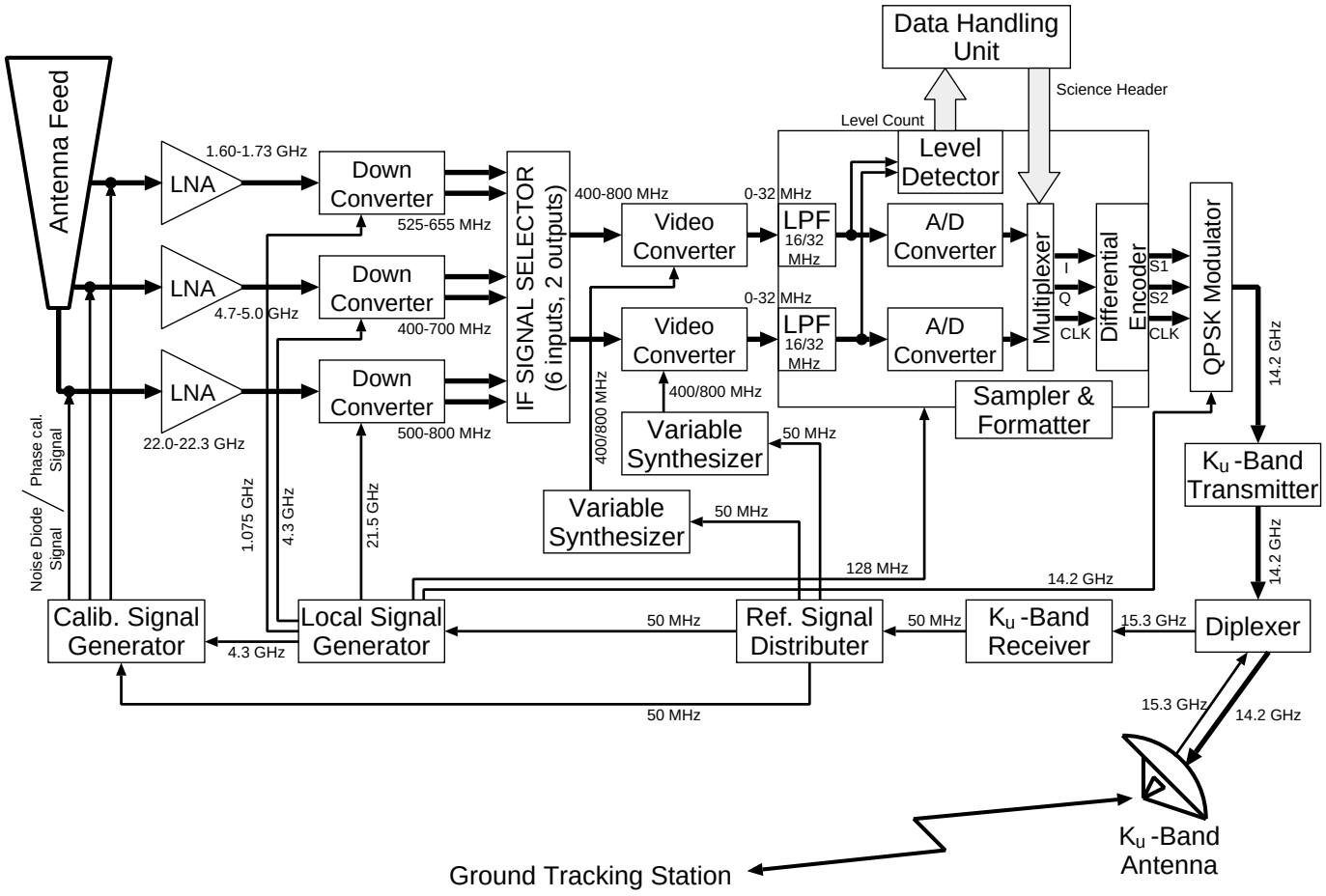

Figure 2: Diagram of the HALCA science subsystem.

determined. Experience has shown that the system temperature and pointing stability of HALCA are very good which means that there has been little difficulty in determining the amplitude calibration for HALCA.

By default, phase calibration tones every MHz throughout the observing band are continuously switched on for continuum observations and switched off for spectral line observations. PIs can request on the VSOP proposal Cover Sheets that the tones be either switched on or off. Both the noise diode and phase calibration signals are injected through 25 dB couplers into the LNAs (see §10 for more details on HALCA data calibration). The phase calibration tones are extracted at the tracking stations.

The properties of the HALCA antenna and science subsystem are summarized in Table 1. The three VSOP observing modes are shown in Table 2. It is important to note that only one of the three observing modes is VLBA/MkIV/S2 compatible (see §8.1 for a discussion of the different VLBI recording systems that will be supporting VSOP observations). It is only this observing mode that can be used when HALCA is co-observing with non-Japanese ground radio telescopes.

Table 1: Properties of the HALCA Science Subsystem

	Observing Band	
	1.6 GHz (18 cm)	5 GHz (6 cm)
Frequency Range (GHz)[1]	1.60–1.73[2]	4.7–5.0
Polarization	LCP only	LCP only
Antenna Efficiency[3]	24%	34%
Antenna Sensitivity (mK Jy^{-1})	4.3	6.2
System Temperature (K)	75	95
SEFD (Jy)[4]	17400	15300

Notes:
1. The frequency range of each channel can be independently set such that the lower and upper frequencies of each channel are an integral number of MHz. The difference between the lower and upper frequencies of each channel must be equal to the channel bandwidth. Thus, for a 16 MHz channel, a frequency range of 1700–1716 MHz is okay, but both 1700.5-1716.5 MHz and 1700–1717 MHz are not.
2. Proposers who wish to observe the 1.72 GHz OH line should be aware that some ground radio telescopes, for example the VLBA, have difficulty supporting observations at 1.72 GHz due to the RFI environment.
3. The HALCA main antenna has a hexagonal shape which has a total area of 50.1 m^2 and is thus equivalent to a circular antenna of diameter 8.0 m. The antenna efficiencies quoted here are based on this area and include the effects of the feed and cable losses described in §3 and are thus not solely a measure of the quality of the antenna. These efficiency values are therefore somewhat lower than the traditionally defined aperture efficiency. Both aperture sensitivity and system temperature are measured at the noise source injection point, near the LNA input and *behind* the coaxial cables that join the feed to the LNAs. See §10 for details.
4. The system equivalent flux density (SEFD), also known as the system temperature in Jy, is the ratio of the system temperature in K to the antenna sensitivity in K Jy^{-1}.

Table 2: HALCA Observing Modes

Mode properties			Recorder compatibility	
Number of channels	Bandwidth per channel	Sampling quantization	VLBA/MkIV/S2 compatible	VSOP terminal compatible
Two	16 MHz	2 bit	yes	yes
Two	32 MHz	1 bit	no	yes
One	32 MHz	2 bit	no	yes

4 HALCA Constraints

HALCA has a number of constraints which may make it impossible for the spacecraft to observe a given source under certain conditions. An understanding of the spacecraft constraints enables the proposer to understand what type of observations are feasible and what time scales are appropriate for monitoring observations.

4.1 Sun

Before the launch of HALCA, it was expected that HALCA could not observe sources within 70° of the sun. This constraint arises from the fact that the solar panels must be fully illuminated by the sun to generate sufficient power for scientific observations. When a source is within 70° of the Sun the main antenna shadows the solar panels; they are therefore under-illuminated and cannot provide the required solar power. However, in-orbit experience has shown that for certain sun angles beyond 70° that the spacecraft experiences larger torques than those predicted before launch. These torques cause the reaction wheels of the attitude control subsystem to absorb more angular momentum throughout an orbit than the maximum design value. (The reaction wheels are unloaded at each perigee by magnetic torquing using the Earth's magnetic field.) Because of this excess torque build up, observations with HALCA had been limited to the sun angle ranges 80-120° and 135–180°. However, this torque build up is now better understood, and consequently the sun angle constraint is being relaxed. Therefore, for observation planning purposes, it is reasonable to assume that HALCA can now observe all sources with sun angles greater than 80°.

Since this constraint refer to the sun it is easiest to understand it in terms of a source's ecliptic latitude (β) and which is related to it's right ascension (α) and declination (δ) as follows:

$$\beta = \sin^{-1}(\cos\epsilon \sin\delta - \sin\epsilon \sin\alpha \cos\delta) \tag{1}$$

where ϵ = obliquity of the ecliptic ($\approx 23.5°$)

A source with $|\beta| > 80°$ is never within 80° of the sun and so is unaffected by this constraint. A source having $|\beta| < 80°$ is unobservable every year for a period ($\Delta t_{\rm unobs}$) of time given by:

$$\Delta t_{\rm unobs} \approx (365/180) \cos^{-1}(\frac{\cos 80}{\cos \beta}) \text{ days} \tag{2}$$

Thus, the maximum length of time a source cannot be observed is 162 days = 4.7 months per year. Such a source lies in the ecliptic plane. Thus, this constraint can have a serious impact on monitoring observations for sources that lie on or near the ecliptic plane.

4.2 Moon

At 1.6 and 5 GHz, HALCA cannot observe sources with 5.0° and 1.8° from the moon's center respectively.

4.3 Earth

Like ground radio telescopes, HALCA cannot observe sources occulted by the Earth. Unlike ground radio telescopes, which are fixed to the Earth, the varying altitude of HALCA means that the fraction of the sky occupied by the Earth varies. At the closest approach of the spacecraft to the Earth (perigee), the Earth occupies 30% of the celestial sphere, whereas at the furthest point from the Earth (apogee) the Earth only occupies 1.3% of the celestial sphere. Thus, this constraint is less severe for HALCA than it is for a ground radio telescope.

4.4 Eclipse

HALCA cannot observe when the Sun is occulted by the Earth or the Moon. When this happens, the spacecraft has to use its batteries for power. Scientific observations are not possible during eclipse because they would cause too large a drain on the batteries. Furthermore, after each eclipse the batteries are re-charged and this battery re-charge time is roughly equal to the eclipse length. During the battery re-charge time it is also not possible to undertake scientific observations. Figure 3 shows the HALCA eclipse history from 1-Jan-2000 to 31-Dec-2001. As can be seen, during this period there are two short periods when there are long eclipses which can last at most $\approx$ 90 minutes. During these short periods of long eclipses no scientific observations will be undertaken.

Eclipses produce gaps in (u,v) coverages that stay fixed from orbit to orbit on the timescale of a typical observation.

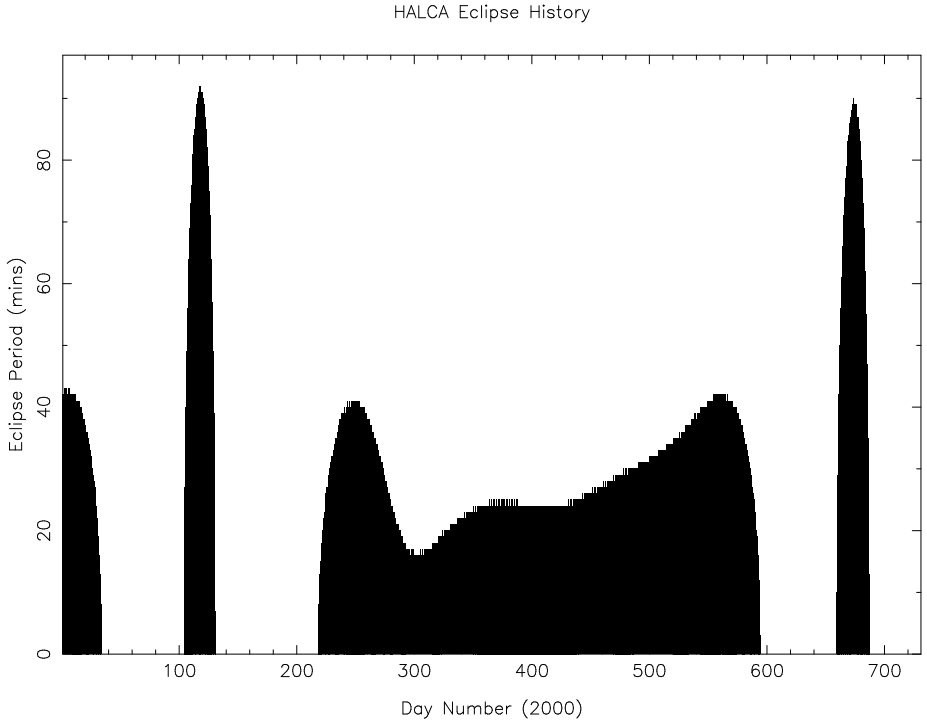

Figure 3: HALCA eclipse history (1-Jan-2000 to 31-Dec-2001).

4.5 Tracking Network

HALCA is supported by a 5-station tracking network (see §6 for more details). The high VLBI data rate (128 Mbps) requires that the VLBI data must be down-linked in real time. Therefore it is impossible for the satellite to observe if it is not above the minimum elevation limit (typically 5°) of any tracking station. In addition, the satellite depends upon contact with a ground tracking station for its local oscillator phase reference.

4.6 Spacecraft Telemetry Horizon Mask

Even if all of the above constraints are met it still may be impossible to observe. HALCA has only one telemetry antenna to transmit the VLBI data to the tracking stations. The telemetry antenna is on a boom attached to the opposite side of the spacecraft main body from the main (8m) antenna. This telemetry antenna itself has a limited field of view, so it cannot communicate with a tracking station

if, from the perspective of the telemetry antenna, the tracking station lies within $\approx 70°$ of the source direction. Thus, in order to communicate with a tracking station, the spacecraft must be above the minimum elevation limit of the tracking station and the tracking station must lie within the field of view of the telemetry antenna.

4.7 Changing Sources

When changing sources, the VSOP satellite can slew at a rate of $2.25°$ min^{-1}. However, slewing is a two-stage process which means that the total angle the spacecraft slews through is greater than or equal to the angle between the two sources. The satellite first slews around the spacecraft-Sun axis followed by a slew about the solar-panel axis. Thus, even under optimum conditions, it takes 80 minutes to slew $180°$. Also, once the slew is completed it takes ≈ 3 minutes for the antenna to settle. Furthermore, HALCA is unable to change sources during eclipse and sufficient star tracker data must be obtained before the attitude is well enough determined before scientific observations may begin. Thus, slewing between sources is a complex procedure and typically takes between 4–10 hours. In general, proposers do not need to worry about spacecraft slewing as this is taken care of during the scheduling of HALCA.

4.8 On-board Command Memory

Once a day (except for Sunday) HALCA receives a new command sequence via the Kagoshima Space Center (see Table 4). This command sequence is composed of at most 256 commands, some of which are devoted to scientific activities. One command is required for each of the following scientific activities: (1) to turn the noise diodes on or off, (2) to change frequency band and/or LO settings, and (3) to change source. Thus there is a trade-off to be made between how frequently to change source, how frequently to change observing band and/or LO settings and how frequently to measure the system temperature. Furthermore it is only possible to observe a maximum of four sources in each command sequence. Although it takes only one command to change source, each source itself requires additional information that is used primarily by the star sensors in the attitude control subsystem.

5 HALCA Orbit

Space VLBI is simply ground VLBI with, in the case of the VSOP mission, an additional antenna in space. Since the science that can be produced by the VSOP mission is intimately tied to HALCA orbit, proposers need to be aware of the basic properties of orbits and how they change with time.

5.1 Definition of the Orbital Elements

To a good approximation, an orbit bound to the Earth is an ellipse with the Earth at one of the foci. It is convenient to refer to the orbit by the properties of this ellipse – the so-called six Keplerian orbital elements. Five of the six elements refer to the properties of the orbit ellipse and its orientation in space. The sixth element determines the location of the spacecraft on this ellipse. These elements, which are defined at a certain epoch, are:

- a: Semi-major axis. The spacecraft orbital period, T, is related to the semi-major axis as follows $\mathrm{T} = 2.76\ (a/10^4\,\mathrm{km})^{3/2}$ hours.
- e: Eccentricity. The distance of the spacecraft from the center of the Earth at the closest approach to the Earth (perigee) is given by $a(1-e)$. The distance of spacecraft at furthest point from the center of the Earth in its orbit (apogee) is given by $a(1+e)$. To calculate the spacecraft height above the surface of the Earth at either perigee or apogee it is necessary to subtract the radius of the Earth from the previous expressions. The orbit semi-minor axis, b, is given by $a\sqrt{1-e^2}$.

Table 3: Nominal HALCA Orbital Elements (Defined at 0 UT on 01-Jan-2000)

Keplerian Orbital Element	Value
a (semi-major axis)	17,356.200 km
e (eccentricity)	0.60480
i (inclination)	31.6600°
Ω (right ascension of the ascending node)	311.4908°
ω (argument of perigee)	43.3615°
M (mean anomaly)	272.7202°
Derived Parameters	
Orbital period	6.32 hours
Apogee height	21,400 km
Perigee height	560 km
Perigee velocity	2.4 km/s
Apogee velocity	9.6 km/s

Note: These orbital elements are those that should be used with simulation software for simulations that cover the third AO period.

i: Inclination. This is defined as $\cos^{-1}(L_z)$, where L_z is the component of the orbit unit angular momentum vector that lies along the Earth's rotation axis. For orbits that lie in the celestial equator (equatorial orbits), $L_z = 1$, and hence $i = 0°$. For orbits perpendicular to the celestial equator (polar orbits), $L_z = 0$ and hence $i = 90°$. HALCA's orbit is inclined 31° to the equator.

Ω: Right ascension (or longitude) of the ascending node. Except for equatorial orbits, a spacecraft crosses the celestial equator twice every orbit: once when it is heading north and once when it is heading south. Ω is the right ascension of the spacecraft when it crosses the celestial equator heading north. This point is known as the ascending node. Like right ascension, Ω is usually measured in hours, but in some circumstances degrees is a more appropriate unit.

ω: Argument of perigee. This is defined as the angle in the orbital plane between the ascending node and perigee as measured from the center of the Earth. When ω is between 0° and 180° the perigee is in the northern hemisphere. Otherwise it is in the southern hemisphere.

M: Mean anomaly. Due to the conservation of angular momentum, the spacecraft moves at a non-uniform rate around the orbit ellipse. The angle between the spacecraft and perigee, as measured from the center of the Earth, is called the true anomaly. However it is convenient to work with another angle called the mean anomaly. If this is measured in degrees, the ratio M/360 is equal to the ratio of the time elapsed since the spacecraft last passed through perigee to the spacecraft orbital period. Thus, for a spacecraft at perigee, $M = 0°$, and for a spacecraft at apogee, $M = 180°$. For a spacecraft in a circular orbit ($e = 0$) the mean anomaly and the true anomaly are the same.

The HALCA orbital elements are shown in Table 3.

5.2 Orbit Normal and (u,v) Coverages

The orientation of the orbital plane in space and the orientation of the orbit semi-major axis within the orbital plane control the type of (u,v) coverage that can be obtained for a given source, provided that the spacecraft constraints can be met. The orbit normal, which lies in the northern hemisphere, and the orbit anti-normal, which lies in the southern hemisphere, define directions along which the highest two-dimensional resolution observations will be obtained i.e., those observations for which the synthesized

beam area is a minimum. The celestial coordinates (α, δ) of the orbit normal and the orbit anti-normal are (Ω−6h, 90°−i) and (Ω+6h, i−90°) respectively. For sources that lie in the orbital plane, that is 90° from the orbit normal, approximately linear (u,v) coverages are obtained.

Figure 4 shows an example of how the (u,v) coverage varies as a function of α and δ at a particular epoch. The case where the source is in the orbit plane can be clearly seen, since this is where linear (u,v) coverage is obtained. The large region with (u,v) coverages that have no space-ground baselines is due to the solar constraint that HALCA cannot observe in the range of sun angles 0°–80°. This region moves with the sun across the sky during the year. More examples of how the (u,v) coverages vary during 2000 and 2001 can be obtained from the following URL:

http://sgra/html_dwm/fakesat_ao3/all_sky.html

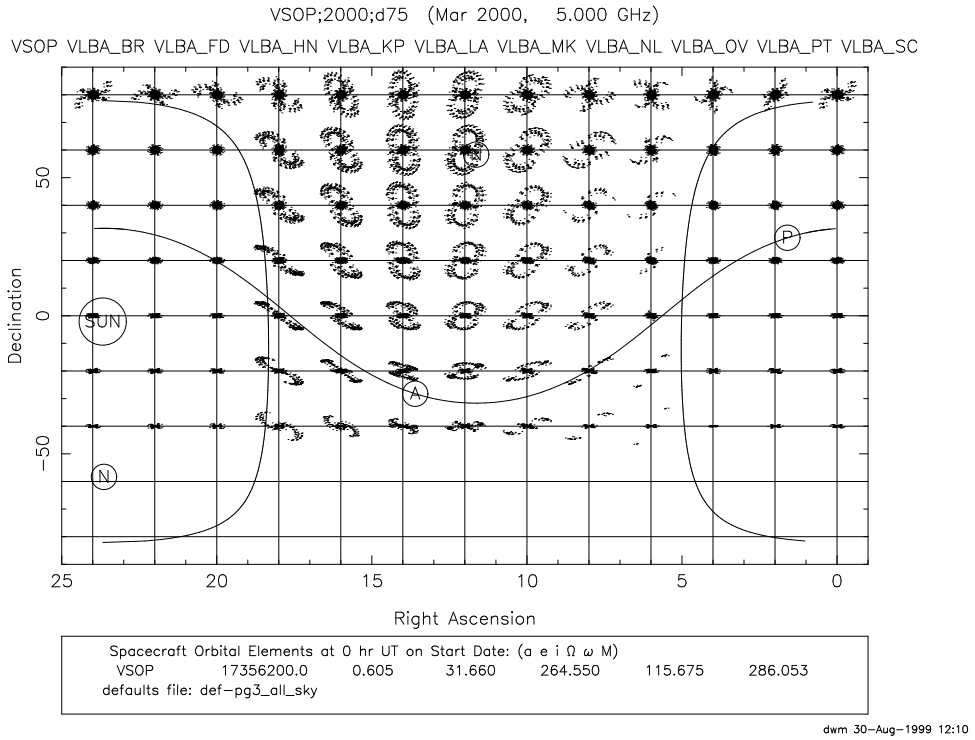

Figure 4: All-Sky (u,v) plot for HALCA with the VLBA on 15 Mar 2000.

At apogee, for a source that lies along the orbit normal direction, the projected baseline lengths range from about 23,000 km to 33,000 km depending on the location of the ground radio telescopes with respect to the spacecraft. Since this lower limit exceeds the maximum baseline that can be obtained with ground-based VLBI arrays ($\approx$ 10,000 km) it inevitably follows that there will be large holes in the (u,v) plane for sources observed along or near the orbit normal (or anti-normal) direction. However, for sources that lie away from the orbit normal direction, the size of these (u,v) holes can be minimized by projection effects. Proposers who want to request specfic observing dates for either single epoch experiments or monitoring experiments can do so in item (11), the 'Additional notes to the scheduler' box on the Cover Sheets.

5.3 Precession of the Orbital Elements

Due to the oblateness of the Earth, the orbital elements ω and Ω precess, which has a significant impact on the (u,v) coverage that can be obtained for a given source as a function of time. These precession rates are given by:

$$\dot{\Omega} = -752 \frac{\cos i}{(1-e^2)^2} \left(\frac{a}{10^4\ km}\right)^{-\frac{7}{2}} {}^\circ\ \mathrm{yr}^{-1} \tag{3}$$

$$\dot{\omega} = -\frac{1}{2}\left(\frac{5\cos^2 i - 1}{\cos i}\right)\dot{\Omega} \tag{4}$$

For the HALCA orbit, $\dot{\Omega} = -231^\circ\,\mathrm{yr}^{-1}$ and $\dot{\omega} = +356^\circ\,\mathrm{yr}^{-1}$.

5.3.1 Impact of Ω Precession

One major consequence of the Ω precession is that the direction of the orbit normal changes with time, and hence the directions in the sky for which the best (u,v) coverages are obtained also change with time. Figure 5 shows an example of how for a particular source, 3C273, the (u,v) coverage varies as a function of time. As can be seen, the (u,v) coverage changes quite dramatically with time.

Plots like those shown in Figure 5 are particularly useful in planning monitoring observations (see §11 on simulation software).

5.3.2 Impact of ω Precession

A major consequence of the ω precession is that the amount of tracking available for HALCA, and hence the amount of space VLBI data that can be obtained during an observation, is a function of ω, and hence the epoch of the observation. The reason for this is that four of the five tracking stations are located in the northern hemisphere (see Table 4). Hence more space VLBI data is obtained when the apogee of the orbit is in the northern hemisphere ($180^\circ < \omega < 360^\circ$) compared to when the apogee is in the south ($0^\circ < \omega < 180^\circ$). See §6 for more details on the tracking network. The relationship between ω and day of the year for 2000 (DOY_{2000}) is as follows:

$$\mathrm{DOY}_{2000} \approx -44.49 + 1.026\,\omega \tag{5}$$

Thus, the best tracking during 2000 is when $\omega = 270^\circ$and hence from the above equation when DOY_{2000} is 233 (20-Aug-2000). Similarly, the poorest tracking occurs when $\omega = 90^\circ$and hence $DOY_{2000} =$ 48 (17-Feb-2000).

Furthermore there is an interaction between the field of view of the VSOP spacecraft telemetry antenna and ω that limits the amount of tracking that is available for certain sources under certain conditions. For example, when apogee is in the northern hemisphere it is difficult to observe far southern sources at or near apogee, since under these conditions the telemetry antenna points away from the Earth and cannot communicate with a tracking station (see §4.6).

Proposers should use the orbit listed in Table 3 when planning what observations are feasible. During the scheduling process, any differences between the nominal and actual satellite orbit will be taken into account when scheduling a particular observation.

6 HALCA Tracking Network

Unlike ground VLBI radio telescopes, for which the hydrogen maser reference signal and VLBI data recorder are typically located close to the antenna, for HALCA these facilities are located at a tracking station many thousands of kilometers from the spacecraft. Two types of tracking stations support HALCA: (1) A single commanding station (S-band) at Kagoshima, Japan, and (2) Five VLBI data acquisition and phase transfer stations (Ku-band). In other parts of this guide the VLBI data acquisition

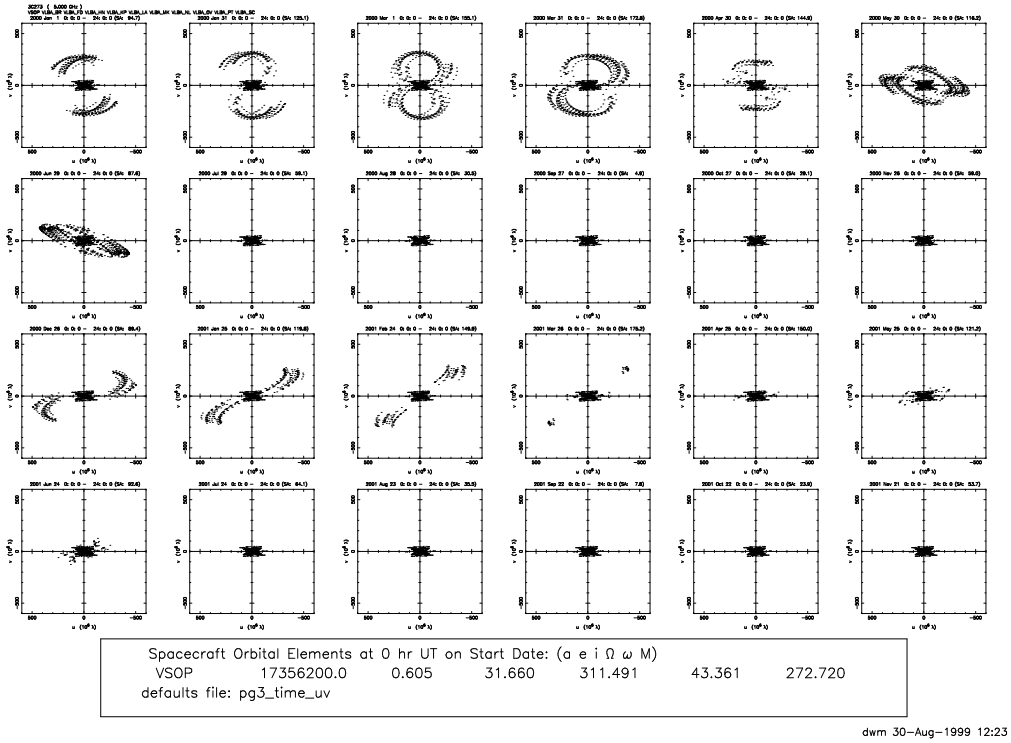

Figure 5: Example (u,v) plot as a function of time. (u,v) coverages for a 14-hour observation of 3C273 with HALCA and the VLBA, starting at the top left on 15 Jan 2000 and going from left to right with a (u,v) coverage produced once a month for a two year period (2000 and 20001). This figure dramatically illustrates the impact of the HALCA solar constraints for sources that lie near or on the ecliptic plane. See Section §?? for more details.

Table 4: HALCA Tracking Network

Location	Code	Latitude	Longitude	Recorder	Agency
Commanding Station (S-band)					
Kagoshima, Japan	-	31° N	131° E	—	ISAS
Tracking Stations (Ku-band) – VLBI Data Acquisition and Phase Transfer					
Usuda, Japan	UZ	36° N	138° E	VLBA/VSOP-T/S2	ISAS
Goldstone, California, USA (DSS-23)	GZ	35° N	116° W	VLBA/S2	NASA/JPL
Robledo, Spain (DSS-53)	RZ	40° N	4° W	VLBA/S2	NASA/JPL
Tidbinbilla, Australia (DSS-33)	TZ	35° S	149° E	VLBA/S2	NASA/JPL
Green Bank, West Virginia, USA	NZ	38° N	80° W	VLBA/S2/VSOP-T	NRAO

and phase transfer stations are simply called tracking stations. Table 4 lists the location of these stations. HALCA is commanded once a day (except for Sunday) from Kagoshima and the international network of 5 VLBI data acquisition tracking stations collect the VLBI data throughout each day. It is important to note that 4 of these 5 VLBI data acquisition tracking stations are in the northern hemisphere. Depending on the time-variable argument of perigee (ω) of the VSOP spacecraft orbit (see §5.3.2), the amount of time that HALCA is above the elevation limits of the VLBI data acquisition tracking stations varies from 55% of the time (for the worst case when $\omega = 90°$) to 85% of the time (for the best case when $\omega = 270°$). The VLBI data acquisition tracking stations record the VLBI data on either VLBA or S2 recorders, with the exception of Usuda which can also record the data on a VSOP terminal (VSOP-T) recorder. After the completion of an observation, the VLBI tapes are shipped to the appropriate correlator. Various auxiliary data are sent to the VSOG, which creates various auxiliary files and sends them to the correlator. These files are needed both for correlation and subsequent data analysis. The VSOG decides which VLBI data acquisition tracking stations track the spacecraft.

7 Ground Radio Telescopes

HALCA is a single element in a VLBI array. Without ground radio telescopes to co-observe with the satellite it is unable to perform its mission. Discussions among the directors of the world's ground observatories, under the auspices of the Global VLBI Working Group (GVWG), have resulted in the telescopes shown in Table 5 being able to participate in space VLBI observations. For each telescope, Table 5 also shows the telescope diameter, the system equivalent flux densities (SEFDs) at 1.6 and 5 GHz, the VLBI recording system (or systems), and the two letter code used to refer to an individual telescope. For comparison purposes the SEFDs for HALCA are shown at the bottom of this table. The system temperatures are the current best estimates and are subject to change.

8 VLBI Recorders and Correlators

8.1 VLBI Recorders

The tracking stations and ground radio telescopes used to support the VSOP mission will use four different recording systems to record the VLBI data. These recording systems are: VSOP-T, VLBA, MkIV and S2. Only one of the three VSOP observing modes, the mode with two 16 MHz two-bit sampled channels (see §3), can be supported by the VLBA, MkIV and S2 systems. All the tracking stations are equipped with both VLBA and S2 recorders. The Usuda tracking station is also equipped with a VSOP-T recorder. These recording systems use different physical media and it is a non-trivial exercise to cross-correlate data recorded on different recording systems with one another except for data recorded on VLBA and MkIV recorders.

8.2 Correlators and Tape Copiers

A comparison of the correlators that are able to support correlation of VSOP data is shown in Table 6. Also shown in the table are the minimum correlator dump time in seconds and the maximum number of frequency channels per 16 MHz per baseline. VLBI experiments using exclusively VLBA and MkIV recording systems are correlated on the VLBA correlator. All other experiments that use either S2 recorders or are mixed-mode, i.e., use more than one type of recorder (with the exception of VLBA and MKIV recorders) are correlated on either the VSOP or Penticton correlators. It should be noted that mixed-mode experiments (again with the exception of those using VLBA and MKIV recorders) require tape-copying before they can be correlated. As shown in Table 7, tape copying facilities are quite limited. There are 2 bi-directional VLBA to VSOP-T tape copying machines and 2 bi-directional S2 to VSOP tape copying machines at the Mitaka correlator. Tape copying is possible at the Usuda tracking station, and is planned for the Green Bank tracking station also.

Table 5: Participating Ground Radio Telescopes and VLBI Networks

GRT/Network	Code[1]	Location	Diam. (m)	SEFD (Jy)[2] 1.6 GHz	SEFD (Jy)[2] 5 GHz	Recorder
Arecibo	AR	Puerto Rico	305	2.5	3.5	S2,VLBA
ATCA (Narrabri)	AT	Australia	6x22	60	80	S2
Ceduna	CD	Australia	30	—	380	S2
EVN:	EVN	Europe/Asia				
Cambridge[3]	CM	UK	32	212	136	VLBA[5], MkIV[4]
Effelsberg	EB	Germany	100	19	20	VLBA, MkIV
Jodrell (Lovell)	JB	UK	76	44	—	VLBA, MkIV[4]
Jodrell (Mk II)	JB	UK	26	—	320	VLBA, MkIV[4]
Medicina	MC	Italy	32	582	296	MkIV
Noto	NT	Italy	32	784	260	VLBA[5], S2
Onsala	ON	Sweden	25	390	600	MkIV
Shanghai	SH	China	25	1088	520	VLBA[5], S2
Torun	TR	Poland	32	200	220	VLBA[5], S2
Westerbork[6]	WB	Netherlands	1x25	280	700	MkIV
Goldstone	GO	USA	70	49	—	MkIV
Hartebeesthoek	HH	South Africa	26	370	680	S2, MkIV
Hobart	HO	Australia	26	1400	1200	S2
Mopra	MP	Australia	22	350	450	S2
Robledo	RO	Spain	70	49	—	MkIV
Tidbinbilla	TI	Australia	70	49	—	MkIV, S2
Usuda	UD	Japan	64	69	69	VSOP-T, S2, VLBA
VLA-27	Y	USA	27x25	14	14	VLBA
VLBA:	VLBA	USA				
Brewster	BR	USA	25	300	290	VLBA
Fort Davis	FD	USA	25	300	290	VLBA
Hancock	HN	USA	25	300	290	VLBA
Kitt Peak	KP	USA	25	300	290	VLBA
Los Alamos	LA	USA	25	300	290	VLBA
Mauna Kea	MK	USA	25	300	290	VLBA
North Liberty	NL	USA	25	300	290	VLBA
Owens Valley	OV	USA	25	300	290	VLBA
Pie Town	PT	USA	25	300	290	VLBA
Saint Croix	SC	USA	25	300	290	VLBA
Spacecraft						
VSOP	—	in orbit	8	17400	15300	—

1. The two letter codes used to represent individual telescopes with the exception of the codes VLBA and EVN that indicate the entire VLBA or EVN arrays that operate at a given frequency. These code letters must be used when specifying ground arrays of individual telescopes or the VLBA and EVN arrays in the VSOP proposal Cover Sheets.
2. The system equivalent flux density (SEFD), also known as the system temperature in Jy, is the ratio of the system temperature in K to the antenna sensitivity in K Jy^{-1}.
3. Cambridge is available for VLBI only during joint EVN/MERLIN sessions.
4. The Cambridge, Lovell, and MK II telescopes all share both a VLBA and MkIV recorder. The default usage is for the MkIV recorder to be used by the Lovell or Mk II telescopes and the VLBA recorder is used with the Cambridge telescope.
5. The Noto, Shanghai, Torun, and Cambridge VLBA recorders are expected to be upgraded to MkIV recorders by the end of 1999.
6. Until the fourth quarter of 2000, HALCA observations will use only a single Westerbork dish. After that time, it should be possible to make tied-array observations using 12 of the 14 dishes that make up the array. In this case, the SEFD values at 1.6 GHz and 5 GHz will be 30 Jy and 70 Jy respectively.

Table 6: Correlator Properties

Correlator	Location	Stations	Format	Min data dump time (seconds)	Max number of frequency channels /16 MHz/baseline
VLBA	Socorro, NM, USA	20	VLBA/MkIV	0.131	1024
VSOP	Mitaka, Japan	10	VSOP-T	0.025	4096
Canadian S2	Penticton, BC, Canada	6[1]	S2	0.001[2]	8192[3]
JIVE	Dwingeloo, Netherlands	16	MkIV/VLBA	1	1024[4]

Table 7: Tape Copiers at the VSOP Correlator

Copier			Number
VLBA	$\leftrightarrow$	VSOP-T	2
S2	$\leftrightarrow$	VSOP-T	2

1. Increase to 7-stations is planned. More than 6-stations can be processed with multiple automatic correlation passes.
2. See §9.12 for more details.
3. Very high spectral resolution is possible, using a digital zoom filter, see §9.11 for more details.
4. Actual number depends on exact experiment configuration. For example, 4096 frequency channels per 16 MHz per baseline are possible for an 8-station observation.

The Joint Institute for VLBI in Europe (JIVE) has built a 16 station MkIV correlator. This correlator may become operational for space VLBI observations at the end of 2000, and if this is the case will be used to correlate VSOP experiments involving the EVN. In general, NRAO has committed the VLBA correlator to processing experiments involving NRAO telescopes, including the VLBA and the VLA.

There is no requirement for PIs to be present during correlation. The PI is sent the correlated VLBI data on either Exabyte or DAT tape and the necessary telescope calibration files are either attached to the correlated data or can be obtained by ftp from the the same ftp servers that are used for ground-based VLBI experiments. Additionally HALCA calibration files are placed on a ftp server at ISAS. For more details on how to obtain the calibration files consult the URL:

http://www.vsop.isas.ac.jp/obs/GRTcal.html

For experiments correlated with the VLBA correlator, the calibration data for the VLBA antennas, the VLA and Effelsberg will be included on the VLBI data distribution tape. The PI can select the medium for their correlated data when the ground radio telescope schedule files are made. Experiments are typically correlated in less than 30 days after the experiment has taken place since there is a finite tape pool and tapes must be recycled in a timely fashion. After correlation has been judged complete and correct at a correlator, the tapes are erased and re-used. The PI has no option to ask that the raw tapes be kept until final data analysis is complete.

9 Observational Capabilities of the VSOP Mission

In this section the proposer is provided with the necessary information to calculate the resolution, the baseline sensitivity, the image sensitivity, and the field of view that one can obtain with VLBI observations using HALCA and co-observing ground radio telescopes. There is also a discussion of the polarization, spectral line, and pulsar observing capabilities of the VSOP mission.

The VSOP mission has been producing high-quality VLBI data for over two years. As an example of the images that can be produced, we show in Figure 6 a comparison of the ground-only

(VLBA+Effelsberg) and ground-space (VLBA+Effelsberg+HALCA) 5 GHz images from a 12-hour VSOP observation of the quasar 1928+738 in August 1997. The associated (u,v) coverage is shown in Figure 7.

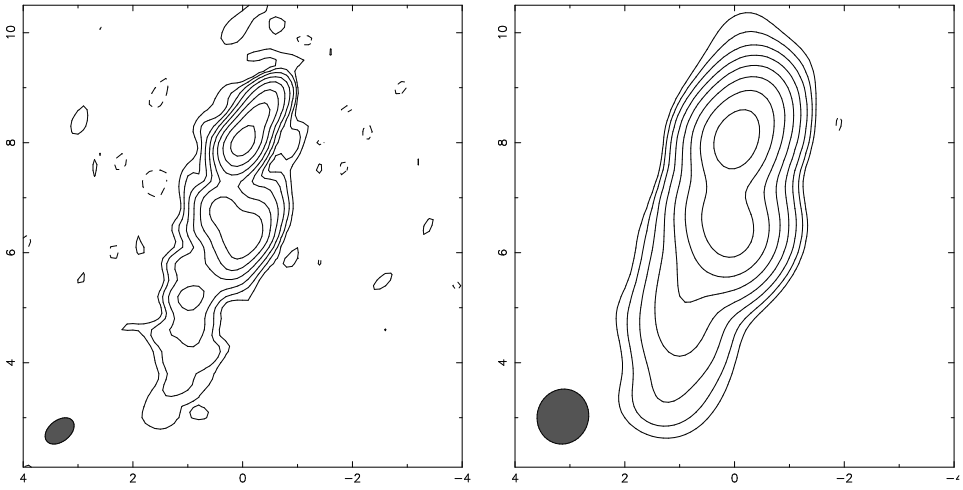

Figure 6: Comparison of ground-space and ground-only 1928+738 images.
Left: ground-space (VLBA+Effelsberg+HALCA) 5 GHz image of 1928+738 from 1997, August 22. Contour levels are -0.5, 0.5, 1, 2, 4, 8, 16, 32, and 64% of the peak, 0.939 Jy/beam. Beam FWHM, 0.598×0.388 mas at $-52°$.
observation.

Right: ground-only (VLBA+Effelsberg) 5 GHz image of 1928+738 at 5 GHz from 1997, August 22. Contour levels are -0.5, 0.5, 1, 2, 4, 8, 16, 32, and 64% of the peak, 1.33 Jy/beam. Beam FWHM, 1.01×0.936 mas at $-17.9°$.

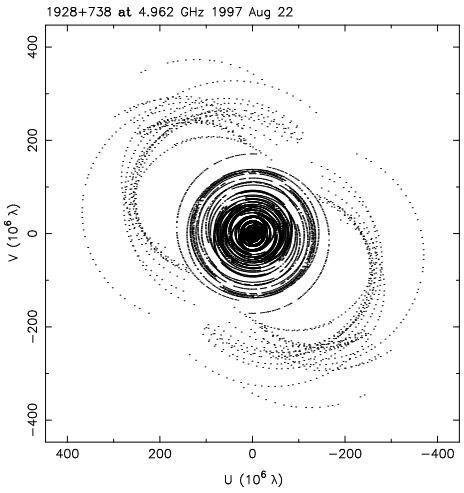

Figure 7: (u,v) coverage for 1928+738 observation with VLBA+Effelsberg+HALCA on 22 August 1997

More examples of images made with HALCA can be found in Hirabayashi *et al.* (1998) and at the URL:

http://www.vsop.isas.ac.jp/general/Images.html

9.1 Resolution

The resolution for an observation depends on the orientation of the source with respect to the orbit normal. For a source that lies along the direction of the orbit normal (or anti-normal), the full width half maximum (FWHM) beam size along the direction of the beam minor axis, $\theta_{\rm minor}$, is related to the observing frequency, ν, as follows:

$$\theta_{\rm minor} \approx 1.2 \left(\frac{\nu}{GHz}\right)^{-1} \text{mas} \tag{6}$$

Similarly the FWHM beam size along the direction of the beam major axis, $\theta_{\rm major}$, is related to the observing frequency, ν, as follows:

$$\theta_{\rm major} \approx 2.3 \left(\frac{\nu}{GHz}\right)^{-1} \text{mas} \tag{7}$$

For sources that do not lie along the orbit normals, the FWHM major and minor beam sizes will be greater than or equal to the values quoted above. Furthermore the above beam sizes are those for an observation with HALCA and the VLBA using uniform weighting with each visibility weighted by the RMS noise level to the power $-\frac{1}{4}$. The beam size is a function primarily of the orientation of the source with respect to the orbit normal and the weighting scheme used. It depends only secondarily on the ground array used. It should also be noted that the FWHM minor axis beam size quoted above is 65% of the size of the fringe spacing for the longest baseline. This is quite consistent with the weighting scheme used.

Example: For a HALCA observation at 5 GHz, in the direction of the orbit normal, $\theta_{\rm minor} = 0.24$ mas and $\theta_{\rm major} = 0.46$ mas.

9.2 Baseline Sensitivity

The RMS thermal noise (σ_{ij}) in the visibility amplitude of a single polarization on a baseline between the i-th and j-th antennas in a VLBI array is given by:

$$\sigma_{ij} = (\eta_s^{-1}) \sqrt{\frac{T_i(Jy) T_j(Jy)}{2B\tau}} \tag{8}$$

where:

η_s = The VLBI system efficiency factor (always < 1). This factor accounts for losses in the VLBI system (e.g. quantization in the data recording and correlator approximations). For 1-bit (2 level) sampling the VLBI efficiency factor is 0.64 while for 2-bit (4 level) sampling this factor is 0.88 (assuming that correlator losses are small).

$T_i(Jy)$ = The SEFD (system temperature in Jy) for the i-th antenna. See Table 5 for the value of this parameter.

$T_j(Jy)$ = The SEFD (system temperature in Jy) for the j-th antenna. See Table 5 for the value of this parameter.

B = The bandwidth in Hz. Theoretically for VSOP continuum observations the value of this parameter is either 32 or 64 MHz (see Table 2 for more details). In practice, it maybe more appropriate to use 16 MHz in fringe fitting SNR calculations for the VSOP observing mode that is compatible with all recording terminals since typically data from each 16 MHz baseband channel is independently fringe-fitted.

τ = The integration period in seconds. For fringe-fitting calculations, τ is the fringe-fitting interval. This should be about equal to the coherence time. See Table 8 for estimated values of the coherence time. For visibility data, τ is the integration period of each visibility point. This integration period can be, and often is, smaller than the coherence time.

Example: At 5 GHz, σ_{ij} is 21 mJy for HALCA to a single 25m VLBA antenna (assuming $T_{\rm HALCA}$ = 15300 Jy, $T_{\rm VLBA}$ = 290 Jy, B = 16 MHz, τ = 400 s and $\eta_s = 0.88$).

Example: At 5 GHz, σ_{ij} is 6 mJy for HALCA to the 100m Effelsberg antenna (assuming $T_{\rm HALCA}$ = 15300 Jy, $T_{\rm Effelsberg}$ = 20 Jy, B = 16 MHz, τ = 400 s and $\eta_s = 0.88$).

Table 8: HALCA (90%) Coherence Times (τ)

Observing Band	1.6 GHz	5 GHz
τ (seconds) ($>$ 1 hour from perigee)	~600	~400
τ (seconds) ($<$ 1 hour from perigee)	~400	~150

9.3 Fringe Fitting Signal to Noise Ratio

When fringe fitting VLBI data, the signal to noise ratio (SNR) on the baseline between the i-th and j-th telescopes in a VLBI array, SNR$_{ij}$, is given by:

$$\mathrm{SNR}_{ij}(\tau) = \frac{C(\tau) S_c}{\sigma_{ij}(\tau)} \qquad (9)$$

where $C(\tau)$ is the coherence function, S_c is the correlated flux density of the source and $\sigma_{ij}(\tau)$ is the RMS noise level, given by Equation 8. Over the fringe-fitting interval, τ, the amplitude of the correlated signal is degraded due to atmospheric irregularities and noise in the frequency standards or in the case of HALCA un-modeled accelerations. C(τ) measures this degradation. To obtain the highest signal to noise when fringe fitting, the fringe fitting interval needs to be chosen such that the SNR, given by Equation 9, is a maximum. A reasonable choice of τ is that for which C(τ) = 0.9. Table 8 shows the values of this interval as measured at the VLBA correlator. For more details about the coherence values in the Table 8 please consult the memo by Ulvestad, 1998 (http://www.nrao.edu/space_vlbi/aoc/vtrep/halca_coher.ps). As can be seen the coherence time is reduced when HALCA is within a hour of perigee passage. Note that Equation 9 requires that the correlated flux density be used and not the total source flux density. Section 9.5 gives a method of how the correlated flux density can be predicted for Earth-space baselines.

Example: At 5 GHz, the SNR is 24 between HALCA and a single VLBA antenna for a 1 Jy circular Gaussian source with a brightness temperature of 1.22×10^{12} K observed on a projected baseline of

25,000 km (assuming $T_{\rm HALCA}$ =15300 Jy, $T_{\rm VLBA}$ = 290 Jy, B = 16 MHz, τ = 400 s, $C(\tau)$ = 0.9, and η_s = 0.88). See Equation 14 for how to calculate the correlated flux density.

Example: At 5 GHz, the SNR is 90 between HALCA and the 100m Effelsberg antenna for a 1 Jy circular Gaussian source with a brightness temperature of 1.22×10^{12} K observed on a projected baseline of 25,000 km (assuming $T_{\rm HALCA}$ =15300 Jy, $T_{\rm Effelsberg}$ = 20 Jy, B = 16 MHz, τ = 400 s, $C(\tau)$ = 0.9, and η_s = 0.88). See Equation 14 for how to calculate the correlated flux density.

9.4 Fringe Detection Limit

One important step in the processing of VLBI data after correlation is that the data must be fringe fit. In fringe fitting data, for ground-based VLBI, a search is made in delay and delay-rate space to find the fringe. For Space VLBI it may also be necessary to search in the delay-acceleration dimension as well, although the fringe fitting of in-orbit-checkout data obtained on the VSOP baselines has not required acceleration searches. If the search space is large then a high minimum SNR is required to guard against the probability of false fringe detection. For space VLBI the size of the search space is critically dependent on the size of the position, velocity and acceleration errors in the HALCA orbit. Experience has shown for a VLBI experiment with HALCA , a reasonable practical constraint on the minimum SNR useful for detecting fringes on the baselines to HALCA is:

$$\boxed{\mathrm{SNR}_{\rm min} \sim 5 - 8} \qquad (10)$$

However, it is strongly recommended that, during data reduction, the user attempt many fringe-fitting trials while varying $\mathrm{SNR}_{\rm min}$, to determine an empirical value which is optimal for the array, source, and experimental setup particular to the observation in question. In certain circumstances using baseline stacking in fringe-fitting it is possible with due care and diligence to increase the signal from HALCA. The minimum SNR can be reduced by using narrower delay and rate search search windows. However, it is recommended that proposers use the above limit when trying to estimate the fringe detection limit on baselines to HALCA. Proposers need to convince themselves and the Scientific Review Committee that there is reasonable chance that SNR_{ij} will exceed $\mathrm{SNR}_{\rm min}$ on baselines to HALCA having projected lengths of order 25,000 km.

9.5 Estimated Correlated Flux Density

The SNR formula (Equation 9) requires that the correlated flux density, S_c, be used. Except for a point source, the correlated flux density is always less than the total flux density of the source. Thus, in order to predict if fringes will be detected on baselines to HALCA, we need a method of predicting the correlated flux density on these baselines. In the two methods described below, we treat the source as a single Gaussian component. In reality it is known that VLBI sources in general have complex morphology. Therefore the methods described below should be applied to the most compact VLBI component in a VLBI source, which for most extragalactic sources is the radio core.

9.5.1 Using the Source Size

If we assume that the source has a circular Gaussian brightness distribution, then the correlated flux density, S_c, measured on a projected baseline of length D is related to the total source flux density, S_0, and the full width half maximum size of the source, θ_{FWHM}, as follows:

$$\boxed{S_c = S_0 e^{-0.093(\frac{D}{10^4\ km})^2(\frac{\theta_{FWHM}}{1\ mas})^2(\frac{\nu}{1\ GHz})^2}} \qquad (11)$$

Example: At 5 GHz, the correlated flux density is 0.56 Jy for a 1 Jy circular Gaussian source with $\theta_{FWHM} = 0.2$ mas observed on a projected baseline length of 25,000 km.

9.5.2 Using the Source Brightness Temperature

A useful way to characterize the monochromatic surface brightness of a radio source is to determine the physical temperature that a black body radiator would need to possess to produce the same observed surface brightness. This temperature is known as the brightness temperature of the radio source. For a circular Gaussian source the maximum brightness temperature, T_b, is related to the component flux density, S_0, the component full width half maximum size, θ_{FWHM}, and the observing frequency, ν, as follows:

$$T_b = 1.224 \times 10^{12} \left(\frac{S_0}{1\,Jy}\right) \left(\frac{\theta_{FWHM}}{1\,mas}\right)^{-2} \left(\frac{\nu}{1\,GHz}\right)^{-2} \text{K} \tag{12}$$

Example: At 5 GHz, the brightness temperature is 1.22×10^{12} K for a 1 Jy circular Gaussian source with $\theta_{FWHM} = 0.2$ mas.

Alternatively if the source brightness temperature is known and the source is again assumed to be a circular Gaussian, Equation 12 may be inverted to solve for the component full width half maximum size, θ_{FWHM}, in terms of the maximum brightness temperature, T_b, the component flux density, S_0, and the observing frequency, ν, as follows:

$$\theta_{FWHM} = 1.106 \left(\frac{S_0}{1\,Jy}\right)^{\frac{1}{2}} \left(\frac{T_b}{10^{12}\,K}\right)^{-\frac{1}{2}} \left(\frac{\nu}{1\,GHz}\right)^{-1} \text{mas} \tag{13}$$

Assuming a circular Gaussian source brightness distribution, the correlated flux density, S_c, is related to the brightness temperature, T_b, projected baseline length, D, and the observing frequency, ν, as follows:

$$S_c = S_0\, e^{-0.114 \left(\frac{S_0}{1\,Jy}\right) \left(\frac{D}{10^4\,km}\right)^2 \left(\frac{T_b}{10^{12}\,\text{K}}\right)^{-1}} \tag{14}$$

Example: At 5 GHz, the correlated flux density is 0.56 Jy for a 1 Jy circular Gaussian source with a brightness temperature 1.22×10^{12} K observed on a projected baseline of 25,000 km.

The equations presented above (11 and 14) should not be taken as the definitive answer of what the correlated flux density will be on baseline lengths exceeding an Earth diameter. These equations are if anything a conservative approximation. Results from the TDRSS space VLBI experiments (Linfield *et al.*, 1989 and Linfield *et al.*, 1990) and ground-based VLBI have shown that a common property of radio sources is that they often have more correlated flux density on long baselines than is obtained by extrapolating simple Gaussian models derived from short baseline data.

9.6 Field of View

The field of view of a space VLBI observation, practically speaking, is limited by two effects which are examined in the following subsections. A third limitation, an effect of non-coplanar phase residuals, will typically be measured in arcseconds for space VLBI observations and is, therefore, insignificant.

9.6.1 Bandwidth Smearing

Due to the finite observing bandwidth, the visibility amplitude of a point source not located at the phase center is degraded. In order that this degradation is limited to only $P\%$, the limit on the field of view, θ_B, that is a function of both the observing bandwidth, B, and the baseline length, D, is as follows:

$$\theta_B = 60\ P^{\frac{1}{2}}\left(\frac{B}{16\ MHz}\right)^{-1}\left(\frac{D}{10^4\ km}\right)^{-1}\ \text{mas} \tag{15}$$

Example: If the visibility amplitude is to be degraded by less than 5%, the field of view is limited to less than 54 mas by this effect for an observation with a bandwidth of 16 MHz on a baseline of 25,000 km.

9.6.2 Time Average Smearing

Due to the finite integration time of each visibility point, the visibility amplitude of a point source not located at the phase center is degraded. Fundamentally, it is the correlator dump time ($\sim$ 1 second) that limits the field of view due time-average smearing. However, it is fairly common practice to time average the visibility data before imaging the data. It is this time averaging of the data that may place a stricter limit on the field of view than bandwidth smearing depending on what visibility averaging time is used.

The general analysis of time average smearing for ground VLBI is difficult and is often restricted for simplicity to a source located at the north (or south) pole. For space VLBI there is an analogy to the ground north pole case, and that is to consider a source located along the orbit normal. Due to the different spacecraft velocities at apogee and perigee, the fields of view are different at these two locations and we will consider both cases. The spacecraft velocity at apogee, v_a, and at perigee, v_p, depend on the spacecraft orbital period, T, orbit eccentricity, e, and orbit semi-major axis, a, as follows:

$$\mathrm{v}_a = \frac{2\pi a}{T}\sqrt{\frac{(1-e)}{(1+e)}}\ \text{and}\ \mathrm{v}_p = \frac{2\pi a}{T}\sqrt{\frac{(1+e)}{(1-e)}} \tag{16}$$

Example: v_a and v_p are 2.4 kms^{-1} and 9.6 kms^{-1} respectively for the nominal VSOP spacecraft orbit listed in Table 3.

In order that the visibility amplitude degradation due to time average smearing is limited to only P%, the limit on the field of view at either apogee or perigee, θ_τ, is a function of the observing frequency, ν, the visibility averaging time, τ_v, and the spacecraft velocity, v, is as follows:

$$\theta_\tau = 96\ P^{\frac{1}{2}}\left(\frac{\nu}{1\ GHz}\right)^{-1}\left(\frac{\mathrm{v}}{1\ kms^{-1}}\right)^{-1}\left(\frac{\tau_v}{100\ sec}\right)^{-1}\ \text{mas} \tag{17}$$

Thus, the field of view can be increased by reducing the visibility averaging time.

Example: If the degradation to the visibility amplitude is to be less than 5%, the field of view is limited to be less than 65 mas at apogee for a visibility averaging time of 30 seconds at 5 GHz. The corresponding limit on the field of view at perigee is 20 mas.

Thus, there is a stricter limit on the field of view for data taken near perigee compared to apogee. Simply stated the field of view due to time average smearing is roughly 10 times smaller for observations with HALCA than with ground-based VLBI due to the high velocity of HALCA at perigee.

9.7 Imaging Sensitivity

Proposers wishing to make images need to work out if the expected RMS noise level on their images is low enough for them to meet the scientific goals of their experiment.

The RMS noise per beam on an image (for natural weighting), ΔI, is given by:

$$\Delta I = \frac{\sqrt{\sum w_{ij}^2 \sigma_{ij}^2}}{\sum w_{ij}} \tag{18}$$

where the summation is over all the visibilities in the experiment and w_{ij} is the weight attached to each visibility point and σ_{ij} is the RMS noise level on the visibility amplitude given by Equation 8. For a VLBI array of equal elements, it is easy to show that:

$$\Delta I = \frac{\sigma_{ij}}{\sqrt{N}} \tag{19}$$

where N is the number of visibility points and σ_{ij} is again the RMS noise level on the visibility amplitude. For an observation of a circumpolar source with an array of equal elements the above equation can be re-expressed in terms of the SEFD of an individual array element, T_i, the length of the observation, τ_{obs}, the bandwidth, B, the number of telescopes in the array, n_t, and the VLBI system efficiency factor, η_s, as follows:

$$\Delta I = \eta_s^{-1} \frac{T_i}{\sqrt{n_t(n_t-1)B\tau_{obs}}} \tag{20}$$

Example: At 5 GHz, for a VLBA-only (n_t=10) experiment on a circumpolar source that lasts 18 hours, ΔI= 25 μJy per beam (assuming $T_{\rm VLBA}$ = 290 Jy, B = 32 MHz and η_s = 0.88).

The extension of Equation 20 to an array of non-equal elements, like the EVN or the addition of HALCA to the VLBA say, is as follows. For such an array we can define a single SEFD number, $< T_i >$, such that the above equation is true for the array, if we substitute $< T_i >$ for T_i. It can be shown that $< T_i >$ is given by:

$$< T_i >= \sqrt{n_t(n_t-1)} \frac{\sqrt{\sum_i \sum_{j \neq i} (T_i T_j)^{1-m}}}{\sum_i \sum_{j \neq i} (T_i T_j)^{-\frac{m}{2}}} \tag{21}$$

In deriving the above expression the weight attached to each visibility point is chosen to be inversely proportional to the RMS noise raised to some power m ($w_{ij} = \sigma_{ij}^{-m}$). For optimum weak source detection $m = 2$. However many VLBI astronomers choose $m = \frac{1}{4}$ for VLBI arrays that contain antennas with a wide range of SEFD values. There is a trade-off to be made for space VLBI as to what is the best value to choose for m. With a lower value of m higher resolution images will be obtained but the beam side-lobe level and the image noise level will be higher. For Figure 6, $m = 0$ was adopted and uniform weighting, as opposed to natural weighting, was used to emphasize the visibilities on the long space baselines, over the higher SNR short baseline visibilities.

Example: For the EVN antennas listed in Table 5 using Equation 21, it can be shown that for m = 1/4, $< T_i >$ is 270 Jy (n_t=9) and 230 Jy (n_t=9) at 1.6 GHz, and 5 GHz respectively. As the number of elements in the EVN array and the $< T_i >$ values are similar to the values for the VLBA the noise level

obtained with a ground observation only with the EVN is similar to what is obtained with the VLBA. The error made by using a simple average for the EVN, $(1/n_t)\sum_i T_i$ as an approximation to $< T_i >$, is to overestimate this value by $\approx 38\%$ and $\approx 18\%$ at 1.6 GHz, and 5 GHz respectively (for $m = 1/4$).

There is a useful extension to Equation 21 and that is to consider the addition of HALCA to a ground array. In that case, the RMS noise level on the image, ΔI_{space}, is related to the RMS noise level obtained with the ground array alone, ΔI_{ground}, as follows:

$$\Delta I_{space} = \Delta I_{ground} \frac{\sqrt{1+\frac{2}{n_g-1}\left(\frac{T_v}{<T_g>}\right)^{1-m}}}{\left(1+\frac{2}{n_g-1}\left(\frac{T_v}{<T_g>}\right)^{-\frac{m}{2}}\right)} \tag{22}$$

where n_g is the number of the antennas in the ground array and $\frac{T_v}{<T_g>}$ is the ratio of HALCA SEFD to the ground array SEFD, calculated using Equation 21. In the above expression the weight attached to each visibility point is chosen to be inversely proportional to the RMS noise raised to some power m ($w_{ij} = \sigma_{ij}^{-m}$).

Example: At 5 GHz for a VLBA experiment with HALCA of a circumpolar source that lasts 18 hours, assuming that the source is always visible for HALCA, $\Delta I_{space} = 25$ μJy per beam for $m = 2$ and 50 μJy per beam for $m = \frac{1}{4}$ (assuming $T_{\rm VLBA} = 290$ Jy, $T_{\rm HALCA} = 15300$ Jy, $B = 32$ MHz, and $\eta_s = 0.88$).

9.8 Dynamic Range

The dynamic range of an image is defined as $P_+/\Delta I_m$, where P_+ is the peak flux density in the image in units of Jy/beam and ΔI_m is the measured RMS noise level on the image also in units of Jy/beam. It should be noted that the definition of dynamic range uses the measured image RMS noise level (ΔI_m) and not the theoretical number (ΔI) calculated using Equation 18. In VLBI images ΔI_m can be significantly higher than ΔI. For example, if the measured noise on the image was equal to the predicted thermal noise then the dynamic range in the previous example for a 1 Jy point source would be $\approx$ 20,000:1. One of the main reasons for this is that the RMS noise level on a visibility point can exceed the thermal noise level predicted by Equation 8 due to systematic amplitude calibration errors. In VLBI amplitudes are typically calibrated to a few percent. Consider the case of an observation of a 1 Jy point source with each visibility point having 5% amplitude errors (1 σ) distributed as a Gaussian about the true 1 Jy value. In this case σ_{ij} would be 50 mJy. For an observation with HALCA and a 10 element ground array for 18 hours the number of visibility points is $\approx 10^4$, assuming a visibility integration period of 350 seconds. Hence according to Equation 19 the RMS noise level on the map is expected to be ≈ 0.5 mJy and the dynamic range is this case would be $\approx$ 2000:1. Calibrating the HALCA antenna is different from what is normally encountered in ground-based VLBI (see §10 for details) and proposers should therefore proceed with caution when estimating the dynamic range that will be achieved. In addition to amplitude calibration errors, the low sensitivity of HALCA baselines and the sometimes poor (u,v) coverage of space VLBI observations may also reduce the achievable imaging dynamic range of space VLBI data. The actual dynamic range achievable may be a factor of 10 worse than predicted by using thermal noise calculations such as Equation 18.

To date, the highest dynamic range of a HALCA image is $\sim$1000:1 for relatively simple core-dominated sources. For sources with complex structure the dynamic range is lower than this by about an order of magnitude. For example, in the 1928+738 example shown is Figure 6 uniform weighting was used and the RMS noise level off-source for the ground-space image is 4.4 mJy/beam which gives a dynamic range for this image of 200:1. However, due to the holes in the (u,v) -coverage, as shown in Figure 7, the 'true' dynamic range on-source will be lower than the off-source value.

9.9 Typical VSOP Observations

Observations in General Observing Time are limited by the length of time the co-observing ground array can observe the source, typically 7–14 hours. Every effort is made to schedule an observation with the best (u,v) coverage that can be obtained on the source given the constraints.

9.10 Polarimetry

Polarimetry observations are possible with HALCA but there are several fundamental, logistical and calibration issues that must be considered when planning such observations. For more details, please consult the web page:

http://www.vsop.isas.ac.jp/obs/Pol.html

Possibilities for achieving reliable polarization calibration for HALCA have been investigated by the VSOP Polarization Study Team and the results are quite encouraging. Based on two experiments conducted in late October 1997, the best estimates of RCP leakage into HALCA's LCP feed are approximately 10% at 5 GHz and 3% at 1.6 GHz. These values were determined using standard calibration procedures and existing software in AIPS. Analysis of later VSOP polariztion experiments will enable the time variability of these leakages to de determined. Thes initial findings of the VSOP Polarization Study Team are described in the following memo (1.05 Mbytes gzipped postscript):

http://www.vsop.isas.ac.jp/obs/pst.ps.gz

9.11 Spectral Line Observations

The type of spectral line VLBI observations that may be conducted with the VSOP mission depend firstly on the properties of the VSOP spacecraft science subsystem, described in §3, and secondly on the properties of the correlator used to correlate the data. In this section we will assume the VSOP spacecraft is operating in the VLBA/MkIV/S2 compatible mode. In this mode the VSOP spacecraft has two 16-MHz channels and it is possible to independently set the frequency range of each of the two channels, provided that the lowest frequency in each channel is an integral number of MHz.

Table 6 compares the properties of the correlators that correlate VSOP observations including the maximum number of frequency channels per 16-MHz per baseline and the minimum correlator dump time or integration period.

For the VLBA correlator, each baseband channel can be resolved into as many as 1024 spectral points, subject to a maximum of 2048 points per baseline, independent of channel bandwidth. For HALCA's fixed 16-MHz channels, the highest velocity resolution will thus be only 3 km/s for OH masers. The output integration time can be any integral multiple of the 131.072-millisecond short-term integration cycle, subject to an overall output data rate limit of 0.5 Mbytes per second.

For the VSOP correlator 8192 spectral line channels per baseline are created and a maximum of 1024 spectral line channels can be output. These output channels can either be individual channels or combinations of channels from the 8192 channel data. Consequently the VSOP correlator can provide a factor of four higher spectral resolution compared to the VLBA correlator. Thus, the velocity resolution with the VSOP correlator for OH masers will be 0.73 $\mathrm{km\,s^{-1}}$. The minimum integration period of the VSOP correlator is 25 milliseconds and the maximum data output rate is 1.5 $\mathrm{Mbyte\,s^{-1}}$.

In a single pass the Penticton correlator can process all baselines with 256 or 512 frequency points per baseline, 12 baselines with 1024 frequency points, 6 baselines with 2048 frequency points, 3 baselines with 4096 frequency points, or 1 baseline with 8192 frequency points. Additionally, the correlator has a decimating digital filter that is used to implement a frequency 'zoom' mode whereby increased spectral resolution can be obtained on a narrower bandwidth. Zoom factors of 4x, 8x, 16x, and 32x can be achieved with a corresponding reduction in available bandwidth. E.g. for a zoom factor of 32, and 2048 frequency points, the usable bandwidth (assuming an input VSOP bandwidth of 16 MHz) is 500 kHz

and the spectral resolution is 244 Hz. The penalty for using zoom mode is a reduction in SNR of 12% due to re-quantization after filtering. More baselines can be processed with high spectral resolution using multiple automatic correlator passes.

To recap the above discussion: If the desired frequency channel bandwidth is greater than or equal to 16 kHz then the VLBA correlator can be used. On the other hand, if narrower frequency channels are desired then the data must be correlated at either Mitaka or Penticton which in turn means that few ground telescopes with either VLBA or MKIV recorders may be used in the experiment due to the limited tape copying facilities.

As with continuum observations, spectral line observers need to convince the Science Review Committee that there is a reasonably good chance of detecting fringes on the baselines to HALCA. In practice this means that the spectral line source has been observed with ground-based VLBI and the correlated flux density on long Earth baselines in known.

9.12 Pulsar Observations

Observations of pulsars with HALCA are possible have already been made during AO1 and AO2. Gating is needed in order to improve the signal to noise of the observations, and is available on the Penticton S2 correlator and the VLBA correlator. Experiments which use the VLBA and other VLBA-format telescopes will be correlated in Socorro. Other experiments using the S2 or VSOP data recording format will be sent to Penticton. For some pulsars between $-20°$ and $-50°$ declination the use of S2 recording telescopes with a few VLBA telescopes would give good (u,v) coverage, but the double copying need from S2 to VLBA is not yet available.

The Penticton S2 correlator has a minimum correlator dump interval of 1.0 milliseconds and at this rate only 6 baselines can be processed at 128 lags (64 frequency points) per baseline. However, this fast dump mode is particularly useful for pulsar observations where it is combined with pulsar gating to keep the total data rate reasonable (e.g. with a gate on time of 10 msec and a period of 100 msec, and a dump time of 1.0 msec, then 100 dumps are generated per second). In fact, this fast dump mode is being used in the V029a Vela pulsar experiment to provide the PI with more information than would be obtained with simple gating. As the dump time increases (2 to 10 msec), the spectral resolution increases as well but still only 6 baselines are available. If the dump time is >= 10 msecs, then more baselines and more spectral resolution are available.

It is important in the correlation of the VSOP data that the correct phasing of the gating is known. If the dispersion of the pulsar is large, the gating time frame versus frequency is also important. Both the Socorro and Penticton correlators do include dispersion in the gating information. The method for obtaining this gating information will depend on the strength of the pulsar and its regularity. For strong pulsars, it may be possible to determine the gating directly from the observations (for example the total power in some of the larger telescopes). For weaker pulsars, special observations (perhaps with other telescopes not involved with the VSOP experiment) may have to be made. Depending on the regularity of the pulsar, these additional observations may have to be made during or within a few days of the HALCA experiment. For some very regular pulsars, no additional observations may be needed.

Contacting the assigned correlator before observation is recommended, in order to determine the method in which the gating information is needed. For the Penticton correlator, please contact Sean Dougherty (Sean.Dougherty@hia.nrc.ca); for the VLBA correlator, please contact Jon Romney (jromney@aoc.nrao.edu).

The processing and imaging of pulsar data, after correlations, should not differ from continuum observations.

9.13 Phase-referencing

In ground VLBI phase referencing—by repointing the antennas every few minutes between the target source and a nearby compact calibrator—the coherence time can be significantly increased with more likely detections of the weak target. Although HALCA has the capability of switching between sources as

close as three degrees, switching times shorter than 30 minutes are not possible for a number of technical reasons. This is far too long for phase connection between the calibrator observations. However, such switching may be useful for a limited number of astrometric programs for which only the delays and rates between the two objects are useful.

Phase referencing when several objects are within the primary beam of HALCA (30′ at 5 GHz, 90′ at 1.6 GHz) may be possible and several experiments are now being analyzed to obtain the source separation for which phase coherence is likely. Because of the orbital errors of >10-meters, large phase errors between objects may occur for separations >3' at 5 GHz and >9' at 1.6 GHz. Please contact the VSOP help facilities before submitting such a proposal.

10 HALCA Calibration

The VSOG is responsible for HALCA calibration and aims to provide a spacecraft calibration file on an observation-by-observation basis that contains all of the relevant information to perform reliable *a priori* calibration and flagging of the HALCA data. This file is in the standard format so that the usual programs used for calibrating VLBI data can be used, such as the UVFLG, ANTAB, and APCAL in AIPS. Production of such files has been subject to delays in the past, however it has been found that the use of the nominal HALCA gain and system temperature data provides a good *a priori* calibration. For further information consult the URL:

http://www.vsop.isas.ac.jp/obs/HALCAcal.html

Similar calibration data for ground radio telescopes will be supplied as is conventionally done with ground-only observations.

11 VSOP Simulation Software

As has been demonstrated in several sections of this guide, VSOP observations with HALCA are quite different from ground-only VLBI. To help potential users better understand the VSOP mission and hence write better proposals, three sets of software have been written to enable proposers to plan experiments. The major difference between the three software packages is the platforms they run on. Software inter-comparisons have shown that the three sets of software give the same correct results for the functions they have in common.
More information on these software packages can be found at the following URLs:

- JPL Fakesat Package (for Unix platforms):
  http://sgra.jpl.nasa.gov/html_dwm/software.html
- SGO (Hungary) Space VLBI Assistance Software (for PCs):
  http://www.sgo.fomi.hu/vlbi/spas.htm
- University of Calgary Space VLBI PC Software:
  http://www.ras.ucalgary.ca/svlbi/software.html

12 VSOP Data Analysis

12.1 Data Reduction

Please consult the following web page for information on how to reduce VSOP data:

http://www.vsop.isas.ac.jp/obs/Reduction.html

12.2 User Support Facilities

There are also several user support facilities around the world where VSOP PIs can obtain help in the analysis of their VSOP experiments. These facilities are described by country or geographic region.

Australia

The Australia Telescope National Facility (ATNF, a division of the Commonwealth Scientific and Industrial Research Organisation, CSIRO), provides regional support for VSOP users based in, or visiting, Australia and the Asia-Pacific region. The ATNF supports reduction and analysis of radio astronomical data at its headquarters at Marsfield, Sydney, through its support scientists and extensive computing facilities. VLBI observations with VSOP and with the Australian Long Baseline Array (LBA) are included in this support.

Canada

Two sites in Canada provide user support for the VSOP mission. The DRAO correlator site at Penticton British Columbia provides consulting to scientists regarding correlator signal processing capabilities to meet specific science requirements. The regional data reduction center at the University of Calgary provides support to scientists regarding data reduction, calibration, and imaging. If desired, PIs may visit the correlator site prior to or during correlation if specific science requirements warrant one-on-one interaction with correlator personnel. Also, PIs may visit the University of Calgary to get assistance with data reduction and imaging.

Europe/China

The Joint Institute for VLBI in Europe (JIVE, Dwingeloo, The Netherlands) provides regional support for VSOP users affiliated with European and Chinese institutes. JIVE support scientists will be available to assist VSOP users at all stages of their VSOP experiments (proposing – scheduling – data reduction). A network of Sun Ultra workstations is available at JIVE for VLBI data reduction and analysis.

Japan

Both the Institute of Space and Astronautical Science (Sagamihara) and the National Astronomical Observatory (Mitaka) are able to support users with assistance from the proposal preparation through to the data reduction. Dedicated computing facilities are available at both locations for fringe-fitting and imaging VSOP data.

United States

The regional user support facility for VSOP PIs based at US institutions is operated by NRAO at the Array Operations Center in Socorro, NM. It includes both expert personnel and high-performance computer hardware. Two scientific staff members supported by NASA, and a third by JIVE, have developed substantial expertise in areas of data analysis specialized for Space VLBI: fringe fitting, calibration, and imaging. It is also possible to reduce VSOP data at NRAO's Green Bank and Charlottesville sites.

13 VSOP Proposal Help

Questions relating to the AO, proposal submission, technical aspects of the mission, or simulation software that are not answered elsewhere in this document or the VSOP Proposer's Guide, may be addressed via e-mail to:

vsop_help@vsop.isas.ac.jp

Such questions will also be compiled to create a 'Frequently Asked Questions' file, which can be accessed on the VSOP WWW site:

http://www.vsop.isas.ac.jp/obs/ObsFAQ.html

Questions directed to the help desk will be responded to in a timely manner. As the resources for proposal support are limited, however, questions should be asked as early in the proposal period as possible, to avoid any possible congestion during the last weeks before the deadline.

14 Web Site for Additional Information

The prime web site for all VSOP related material is the VSOP web site at ISAS:

http://www.vsop.isas.ac.jp

15 Acknowledgments

The original version of the Proposer's Guide included contributions from D. Murphy, P. Edwards, D. Gabuzda, H. Hirabayashi, M. Inoue, H. Kobayashi, D. Meier, G. Moellenbrock, Y. Murata, I. Noszticzius, R. Taylor, J. Ulvestad and A. Wiercigroch.

B. Carlson, P. Edwards, S. Frey, D. Meier, G. Moellenbrock, D. Murphy, J. Romney, R. Taylor and S. Tingay provided material for the revised version of the Proposer's Guide released in conjunction with the second VSOP AO. The second version of the Proposer's Guide has been improved with comments from L. Gurvits, H. Kobayashi, A. Mioduszewski, and R. Preston.

The third version of the Proposer's Guide is a revision of the second version by D. Murphy, P. Edwards, and E. Fomalont.

A References

Hirabayashi, H., Hirosawa, H., Kobayashi, H., *et al.* 1998, Science, 281, 1825 and erratum 282, 1995

Hirabayashi, H. 1999 in "Modern Radio Science 1999", edited by M.A. Stuchly (Oxford University Press) p. 51.

Linfield, R. P., *et al.* 1989, Astrophysical Journal, 336, p. 1105.

Linfield, R. P., *et al.* 1990, Astrophysical Journal, 358, p. 350.

Ulvestad, J. S. 1998. Memo 'VLBA Coherence Measured at the VLBA Correlator'.

B Acronyms and Abbreviations

α	Right Ascension
δ	Declination
ω	Argument of Perigee
Ω	Right Ascension of the Ascending Node
AIPS	Astronomical Image Processing System
A/D	Analog to Digital
ATCA	Australia Telescope Compact Array
ATNF	Australia Telescope National Facility
AO	Announcement of Opportunity
DAT	Digital Audio Tape
DSN	Deep Space Network
EVN	European VLBI Network
FITS	Flexible Image Transport System
ftp	file transfer protocol
FWHM	Full Width Half Maximum
GPS	Global Positioning Satellite
GRT	Ground Radio Telescope
GVWG	Global VLBI Working Group
HALCA	Highly Advanced Laboratory for Communications and Astronomy
IF	Intermediate Frequency
IRM	Image Rejection Mixer
ISAS	Institute of Space and Astronautical Science
JIVE	Joint Institute for VLBI in Europe
JPL	Jet Propulsion Laboratory
LO	Local Oscillator
LCP	Left Hand Circular Polarization
mas	milli-arcseconds
Mbps	Mega bits per second
NAO	National Astronomical Observatory
NASA	National Aeronautics and Space Administration
NRAO	National Radio Astronomy Observatory
PI	Principal Investigator
QPSK	Quadrature Phase Shift Key
RCP	Right Hand Circular Polarization
RCS	Reaction Control Subsystem
RFI	Radio Frequency Interference
RMS	Root Mean Square
SEFD	System Equivalent Flux Density
SNR	Signal to Noise Ratio
TDRSS	Tracking and Data Relay Satellite System
URL	Uniform Resource Locator
VLA	Very Large Array
VLBA	Very Long Baseline Array
VLBI	Very Long Baseline Interferometry
VSOG	VSOP Science Operations Group
VSOP	VLBI Space Observatory Programme

C HALCA Mass and Power Budgets

Table 9: Satellite Mass Budget (kg) from Hirabayashi (1999)

Radio astronomy payload	25.0
Ku-band communication	30.5
Deployable antenna	256.5
GPS receiver	8.6
Electric power	115.3
S-band communication	8.3
Command and data processing	16.4
Attitude and orbit control	80.3
Reaction control system (RCS)	30.0
Launch operation	5.7
Thermal control	19.2
Structure	123.5
Wire harness and others	45.0
Satellite dry mass	764.3
RCS propellant	62.0
Total mass	826.3

Table 10: Satellite Power Budget (W)

	Apogee	Perigee
Science payload	70.7	70.7
Ku communication system	44.3	44.3
Ku antenna	40.0	40.0
Solar panels	2.9	2.9
Power	4.8	4.8
S-band receiver	7.6	7.6
S-band transmitter	12.7	4.6
Command and data handling	15.6	15.6
Inertial reference units	37.3	37.3
Star trackers	69.4	69.4
Reaction wheels	26.4	26.4
Attitude control	10.6	10.6
Momentum unloading	0.0	18.2
GPS	9.7	31.4
Battery heater	29.2	29.2
Reaction control system heater	60.6	60.6
Sum	441.8	473.6
Conversion and other losses	92.5	100.4
Charging	30.2	30.2
Total power consumption	564.5	604.2

D Change Log

In this appendix major changes between versions of the Proposer's Guide released with AO2 (PG2) and AO3 this document (PG3) are itemized.

- Update cover page
- Update §4.1 to reflect relaxation of VSOP solar constraints.
- Update HALCA eclipse history to cover the years 2000 and 20001
- Update HALCA orbital elements in Table 4
- Update all-sky (u,v) coverage example (Figure 4) and discussion in §5.2
- Update time (u,v) coverage figure (Figure 5)
- Update §5.3.2 and Equation 5
- Update ground radio telescope section §7 and in particular Table 5
- Shorten §9.10 and include web links to ISAS polarization web page and to a memo describing the results of the VSOP polarization study team.
- Add sub-section on phase referencing observations (§9.13)
- Remove sections on source selection and scheduling (PG2 §10 and PG2 §11)
- Shorten calibration section and simulation software sections (§10 and §11)
- Shorten sub-section of data reduction (§12.1)
- Shorten section on proposal help (§13)
- Shorten section on web site for additional information
- Replace satellite mass budget table with final version (appendix C)
- Replace All-sky UV-plot examples in appendix D with the changes between PG2 and PG3